

A combined experimental and theoretical investigation of the
Al-Melamine reactive milling system: a mechanistic study towards
AlN-based ceramics

Peer-reviewed author version

Rounaghi, Seyyed Amin; VANPOUCKE, Danny E.P.; Eshghi, Hossein; Scudino, Sergio; Esmaeili, Elaheh; Oswald, Steffen & Eckert, Jürgen (2017) A combined experimental and theoretical investigation of the Al-Melamine reactive milling system: a mechanistic study towards AlN-based ceramics. In: JOURNAL OF ALLOYS AND COMPOUNDS, 729, p. 240-248.

DOI: 10.1016/j.jallcom.2017.09.168

Handle: <http://hdl.handle.net/1942/24896>

**A combined experimental and theoretical investigation of the Al-Melamine reactive
milling system: a mechanistic study towards AlN-based ceramics**

Seyyed Amin Rounaghi^{1,*}, Danny E. P. Vanpoucke^{2,3}, Hossein Eshghi⁴, Sergio Scudino⁵,
Elaheh Esmacili⁶, Steffen Oswald⁵, Jürgen Eckert^{7,8,**}

1) Department of Materials Engineering, Birjand University of Technology, 9719866981 Birjand,
Iran

2) UHasselt, Institute for Materials Research (IMO-IMOMEC), Agoralaan, 3590 Diepenbeek,
Belgium

3) IMOMEC, IMEC vzw, 3590 Diepenbeek, Belgium

4) Department of Chemistry, Faculty of Sciences, Ferdowsi University of Mashhad, 91775-1436
Mashhad, Iran

5) Institute for Complex Materials, IFW Dresden, Helmholtzstraße 20, 01069 Dresden, Germany

6) Department of Chemical Engineering, Birjand University of Technology, 9719866981 Birjand,
Iran

7) Erich Schmid Institute of Materials Science, Austrian Academy of Sciences, Jahnstraße 12, A-8700
Leoben, Austria

8) Department Materials Physics, Montanuniversität Leoben, Jahnstraße 12, A-8700 Leoben, Austria

*) Corresponding author. E-mail address: rounaghi@birjandut.ac.ir

**) Corresponding author. E-mail address: juergen.eckert@unileoben.ac.at

Abstract

A versatile ball milling process was employed for the synthesis of hexagonal aluminum nitride (h-AlN) through the reaction of metallic aluminum with melamine. A combined experimental and theoretical study was carried out to evaluate the synthesized products. Milling intermediates and products were fully characterized via various techniques including XRD, FTIR, XPS, Raman and TEM. Moreover, a Boltzmann distribution model was proposed to investigate the effect of milling energy and reactant ratios on the thermodynamic stability and the proportion of different milling products. According to the results, the reaction mechanism and milling products were significantly influenced by the reactant ratio. The optimized condition for AlN synthesis was found to be at Al/M molar ratio of 6, where the final products were consisted of nanostructured AlN with average crystallite size of 11 nm and non-crystalline heterogeneous carbon.

Keywords: Aluminum/Melamine ratio; Mechanism; Mechanochemical synthesis; Nanostructured aluminum nitride ceramic; DFT calculations.

1. Introduction

Nowadays, the demand for technically important nanoceramics with fascinating properties is quickly growing. However, the use of these nanoceramics is considerably restricted due to some difficulties related to the synthesis of nanoceramics. The main challenges are attributed to the accessibility to the expensive high-tech instrumentations and the low manufacturing yield which hinder large-scale production and increase the costs [1]. Therefore, the development of simple and non-expensive fabrication routes for the high yield preparation of nanoceramics is demanded. Among the various synthetic methods, mechanochemistry is known as a versatile and environmentally friendly approach for the synthesis of nanoceramics at ambient conditions [2, 3]. Mechanochemistry is a branch of chemistry in which chemical reactions are induced through the input of mechanical energy [2, 3]. This approach offers a unique opportunity for the synthesis of organic, inorganic and carbon-based nanomaterials [2-7]. Conventional high-energy ball milling, in which the activation energy is provided by the ball impacts, is frequently used for inducing mechanochemical reactions [8]. The process brings many advantages in comparison to the conventional wet chemical- and thermally-assisted routes, including solvent-free synthesis, increased reaction rates at low temperature, overall simplicity and very low production costs [2, 3].

Among the nanoceramics fabricated by ball milling, nitrides of the group III have attracted significant attention due to their outstanding optical and electrical properties [9]. Nitrides are commercially synthesized by the carbothermal reduction of metal oxides in a flowing N_2/NH_3 gas mixture or through direct nitridation of metals at elevated temperatures [10-13]. Among the nitrides, AlN is of particular interest for electronic applications due to its unique properties, including a large band gap (6.2 eV), a low dielectric constant, high thermal conductivity and a low linear thermal expansion coefficient [11, 14, 15].

The mechanochemical synthesis of AlN has to date consisted of ball milling of Al or Al₂O₃ under N₂ or NH₃ atmosphere [16, 17]. Although the process benefits from a room-temperature solid-state procedure, it still suffers from some serious drawbacks, such as the prolonged milling times and the requirement of pressurized toxic gaseous atmosphere [16, 17]. The substitution of the gaseous atmosphere with a solid source of nitrogen would be a promising noteworthy approach. However, the choice of a proper, safe and non-explosive solid nitrogen-rich compound is challenging. It has been previously demonstrated that solid nitrogen-containing organic compounds (SNCOCs) such as cyanamide [18], dicyanamide [19] and melamine [20] have been feasibly employed for the simultaneous thermal reduction/nitridation of metal oxides. Various metal nitrides have been successfully fabricated at relatively high temperatures through this solid-state technique. Recent investigations revealed that the SNCOCs can be used for the synthesis of nitrides through the ball milling process [21, 22]. In this case, the metal nitride is prepared by the milling of a SNCOC with the corresponding metallic element at room temperature. So far, the synthesis of metal nitrides such as AlN and TiN has been respectively reported through the mechanochemical reaction of Al and Ti with melamine, diaminomaleonitrile and urea [21-23]. Recently, we proposed the first stepwise mechanistic approach for the mechanochemical synthesis of nanostructured AlN through a detailed theoretical and experimental investigation of the Al-melamine system [24]. The results demonstrated that at the stoichiometric reactant ratios, the reaction was mainly governed by the polymerization of melamine and the formation of a carbon nitride (CN_x) phase. However, there is still a lack of knowledge regarding to the mechanochemical nitridation reactions induced by ball milling, the role of reactants ratio on the reaction mechanism and the structural characteristics of final products. The current study aims to investigate the effect of various amounts of reactants on the structures and types of the final products in the ball milling process. Moreover, the optimized experimental conditions for the synthesis of AlN are proposed.

2. Experimental procedures

2-1. Sample preparation

Al (Goodfellow, 99.5 % purity, -120 mesh) and melamine (Khorasan Petrochemical Co., 99.8 % purity, -325 mesh) powders were used as-received without any further purification. The powders were mixed with different Al-to-melamine molar ratios (Al/M) of 2, 4, 6 and 10. In each experiment, 3 g of the powder mixture was loaded into a hardened steel vial along with 10 mm diameter hardened steel balls to give a ball-to-powder weight ratio of 50:1. No additive or process control agent (PCA) was added to the mixture. Charging and discharging of the vials were done in a purified argon-filled glove box (less than 1 ppm O₂ and H₂O) to protect the materials from surface oxidation. Milling experiments were conducted using a Retsch PM-400 planetary ball mill at a rotating speed of 300 rpm. The milling was performed at room temperature for various times. The milling times were adjusted for the samples with various Al/M ratios based on the reaction completion times (monitored by XRD and FTIR).

For the phase characterization of carbonaceous by-product, a small quantity of powder milled for 6 h with Al/M = 6 was added to a 10 M aqueous solution of NaOH and stirred for 2 h at 85 °C. After centrifugation of the suspension, the resulting sediment was stirred again with 37% HCl at room temperature for 1 h. The remaining black particles were removed by centrifugation and washed with distilled water until it reached neutral pH value of 6–7. XRD and Raman measurements were carried out on this sample after overnight drying at 85 °C.

2-2. Materials characterization

X-ray diffraction (XRD) patterns were measured using a Philips X'Pert X-ray diffractometer with Co K α radiation ($\lambda = 0.17889$ nm). Rietveld refinement was used to analyze the crystallite size of the milled products. Fourier transform infrared spectroscopy (FTIR) spectra were

collected at room temperature over the range of 4000-400 cm^{-1} , using a ThermoNicolet Avatar 370 infrared spectrometer with KBr pellet technique. The X-ray photoelectron spectroscopy (XPS) experiments were carried out at room temperature in an ultra-high vacuum system equipped with a SPECS PHOIBOS 100 hemispherical electron analyzer. Raman analysis was performed using a DXR SmartRaman with an exciting laser wavelength of 532 nm and a resolution of 1 cm^{-1} . High resolution transmission electron microscopy (HRTEM) measurements were conducted by a Tecnai F30 (FEI company) microscope, operating at 300 kV.

2-3. Computational details

Ab initio density functional theory (DFT) calculations are performed using the projector augmented waves method, as implemented in VASP. Electron exchange and correlation energies are obtained with the generalized gradient approximation, as proposed by Perdew, Becke and Ernzerhof (PBE). The kinetic energy cutoff was set to 600 eV. The structures were optimized using a conjugate gradient method and the energy convergence criterion was set to $1.0\text{e-}6$. For the molecular calculations, no Van der Waals interactions were included, assuming that the molecules are sufficiently separated in the experiments.

3. Results and discussion

The XRD patterns of powder mixtures milled for various times at different Al/Melamine (Al/M) ratios are presented in Figs. 1a-d. The weak peaks at $30^\circ \leq 2\theta \leq 35^\circ$ arise from the sample holder. It is inferred from the patterns that the final milling product changes by the variation of the Al/M ratio. In the system with $\text{Al/M} = 2$ (Fig. 1a), the peaks indexed to the reactants disappear after 12 h, suggesting that the reaction between Al and melamine has occurred. The peaks appearing at the milling times longer than 18 h are assigned to 2-

cyanoguanidine ($C_2H_4N_4$) which is a dimer of cyanamid. No peaks corresponding to AlN are observed in the patterns (Fig. 1a), probably as a result of very fine crystallite size. However, the formation of AlN in the final product (sample milled for 24 h) is inferred from FTIR analysis, as is shown in the next section.

As the Al/M ratio increases to 4 and 6 (Figs. 1b and c), broad peaks of hexagonal AlN appear and become dominant, implying reaction of the Al particles with melamine and then, the formation of AlN. When the Al/M ratio exceeds 6 (Al/M = 10, Fig. 1d), an aluminum carbonitride (AlC_xN_{1-x}) phase is formed instead of AlN. The chemical composition of this phase was found to be $Al_{10}C_1N_9$, as determined by XPS analysis. Since the carbonitride phase is a nitrogen rich phase, it can be expected that the crystal structure should be similar to hexagonal-AlN. The peak appeared at $2\theta = 52.3^\circ$ in some patterns is ascribed to iron contamination resulted from the milling media. The broad AlN and $Al_{10}C_1N_9$ peaks reveal the nanostructural nature of the synthesized phases. Using Rietveld refinement, the mean crystallite sizes for the final milling products in the systems with Al/M ratios of 4 (milled for 10 h), 6 (milled for 6 h) and 10 (milled for 8 h) are determined to be about 8 ± 1 , 11 ± 1 and 6 ± 1 nm, respectively. The largest size for the sample with Al/M = 6 indicates that the AlN crystallite size becomes smaller when the Al/M ratio deviates from the stoichiometric value.

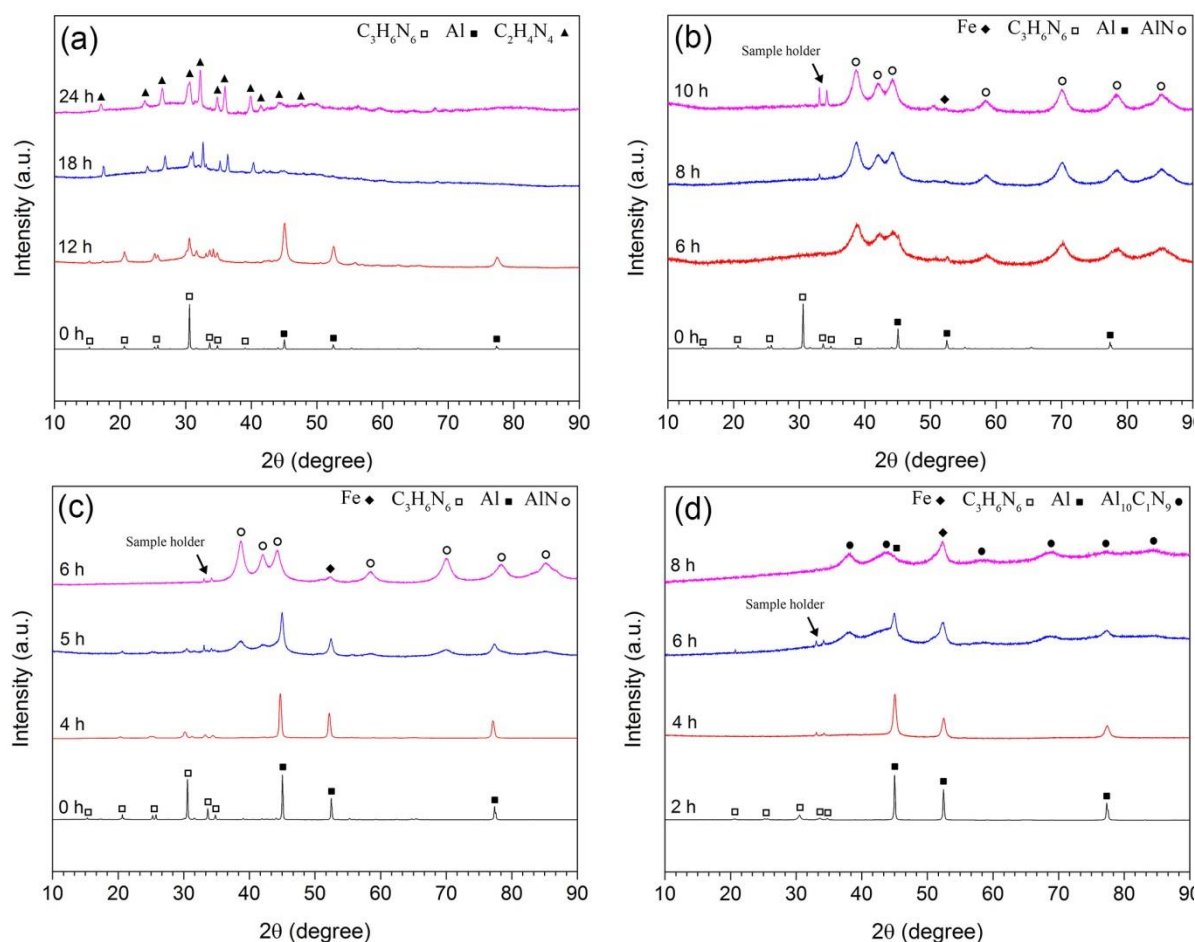


Figure 1. XRD patterns of the powder mixtures with Al/M ratios of a) 2, b) 4, c) 6 and d) 10 milled for various times.

It is also deduced from the XRD results that the reaction time is influenced by Al/M ratio, when the same milling conditions are applied. Indeed, the extended milling times are required for the reaction completion, when the Al/M ratio deviates from the stoichiometric value (Al/M=6). In other words, the deviation of the Al/M ratio from the stoichiometric value dilutes the system by either Al or melamine precursors, which hinders the reaction.

The FTIR spectra of the milled samples with different Al/M ratios are presented in Fig. 2. For comparison, the FTIR spectrum of pure melamine is also provided (Fig. 2a). The peaks at the range of $3000\text{--}3500\text{ cm}^{-1}$ and $1600\text{--}1650\text{ cm}^{-1}$ are respectively attributed to the stretching and bending vibration modes of the amine groups in the melamine molecule. The peaks at frequencies between $1100\text{--}1600\text{ cm}^{-1}$ correspond to the C–N and C=N stretching vibration

modes of the triazine ring. The bands at 450-1050 cm^{-1} are attributed to the C–NH₂ along with the ring vibrations. The peaks presented at 814 cm^{-1} and 1027 cm^{-1} are associated with out-of-plane bending and breathing vibration modes of the triazine ring, respectively.

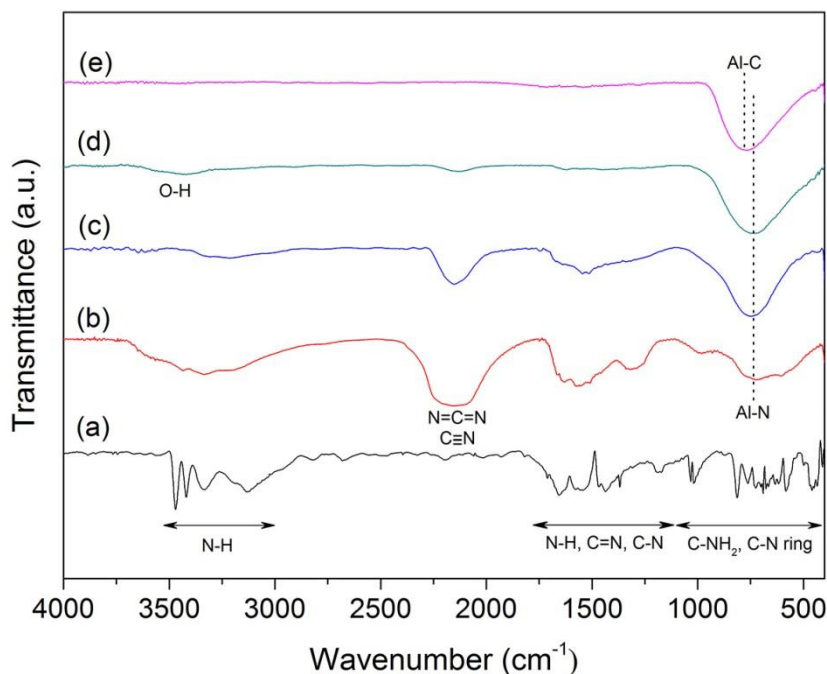


Figure 2. FTIR spectra of a) melamine and milling products with Al/M ratios of b) 2, c) 4, d) 6 and e) 10 milled for 24, 10, 6 and 8 h, respectively.

Fig. 2b presents the FTIR spectrum of the sample with Al/M = 2. In this spectrum, the absence of the characteristic bands of triazine ring at frequencies of about 450-550, 814 and 1027 cm^{-1} and the appearance of the band centered at 720 cm^{-1} respectively point to the dissociation of melamine and the Al–N bond stretching vibrations [25]. This observation fully confirms that nitrogen atoms presented in the melamine molecule partially react with Al, leading to the formation of AlN and melamine fragments. The intense broad band at 2000-2270 cm^{-1} stands for the stretching vibration modes of C≡N (nitrile group) and N=C=N bonds. The appearance of this band together with the broad resonance from 1300-1700 cm^{-1} corresponded to N-H, C=N, and C-N vibrations, is attributed to the characteristic IR modes of 2-cyanoguanidine. The results are in a good agreement with the corresponding XRD pattern in Fig. 1 which confirms

the synthesis of 2-cyanoguanidine during the milling process. The other broad peaks in the range of 3000-3600 cm^{-1} are assigned to the stretching vibration modes of N–H and O–H bonds, respectively arising from the amine groups in 2-cyanoguanidine molecule and the moisture absorption on the powder surface. The IR band features reveal no significant changes for Al/M = 4, suggesting that the reaction pathway and, consequently, the milling products remain approximately unchanged at low Al/M values (Figs. 2b and c). However, compared to Fig. 2b, at larger Al/M ratios (Al/M = 4), the descending propensity of the bands intensity related to the organic constituent and the ascending tendency of the AlN peak intensity are respectively attributed to the consumption of 2-cyanoguanidine and the formation of AlN. In other words, an Al/M ratio of 4 brings more Al particles into the reactant mixture, which subsequently react with more N atoms. This results in the presence of a smaller amount of N-containing species such as 2-cyanoguanidine in the final products. This trend continues until the Al/M ratio reaches up to the stoichiometric value (Al/M = 6) where the characteristic bands of 2-cyanoguanidine disappear and the Al–N peak is dominating (Fig. 2d). In this case, Al particles entirely react with N atoms of melamine and the other reaction intermediates to form AlN. Further increasing the Al content shows no significant changes in the IR band characteristics except a slight shift of the Al–N band towards the higher frequencies (Fig. 2e). This could be ascribed to the chemical structure of the synthesized $\text{Al}_{10}\text{C}_1\text{N}_9$ phase in which the band shift of the AlN peak to 764 cm^{-1} results from the contribution of the stretching vibrations of Al–C bonds (at around 770 cm^{-1} [26]).

The abovementioned FTIR results are corroborated by the XPS data presented in Figs. 3 a and b. The N1s spectrum of the as-received pure melamine shows a specific peak at 398.6 eV assigned to the C–N=C bond of the melamine molecule [27, 28]. Due to the formation of 2-cyanoguanidine at low Al/M ratios (Al/M = 2 in Fig. 3a), the mentioned peak intensity remains more pronounced. However, it gradually disappears for the samples with Al/M ratios exceeding

4. This indicates the consumption of the N atoms with different bonding states in melamine, 2-cyanoguanidine and other C-N containing species. The N1s characteristic peak of Al-N appears at 396.7 eV [29]. The intensity of this peak increases with the increase of Al content until it becomes dominant for Al/M > 4. The broad and weak peak shoulder observed in the N1s spectra of the samples with Al/M = 6 and 10 is attributed to Al-O-N (or C=N-C), NH_x and Al-N-O bonds which form on the surface of the nanostructured AlN as a result of surface oxidation [29, 30]. The observed slight shift of the Al-N peak to 396.2 eV in the N1s spectrum of the sample with Al/M = 10 can be justified by N-N bonded defects on the surface of AlN, which originates from the nitrogen atoms with a coordination number of less than four and/or the incomplete layer formation [29].

The melamine C1s spectrum reveals two distinct peaks at 284.5 eV and 287.5 eV assigned to sp² C-C and N-C=N, respectively [31, 32]. The weak peak at 284.5 eV originates from the incorporation of carbon impurities in the melamine powder. The C1s spectrum reveals no remarkable changes when the Al content is low (Al/M = 2 in Fig. 3b). In this case, the major peak at 287.3 eV is attributed to the N-C=N binding energy of 2-cyanoguanidine molecule. The right peak shoulder observed at around 284.5 eV is assigned to sp² C-C, which is pronounced in comparison to the corresponding C1s spectrum of pure melamine. This probably results from the carbonaceous by-product formed through the dissociation of melamine and the reaction of N atoms with the Al particles. For Al/M > 2, the peak at 287.5 eV (N-C=N) gradually disappears and the peak at 284.5 eV (sp² C-C) starts to be dominant. The increase of the Al content results in higher consumption of N atoms through the nitridation reaction which, in turn, causes more carbonaceous species to be formed. This trend continues until the Al/M ratio reaches the stoichiometric value (Al/M = 6), where the Al particles entirely react with N atoms to form AlN (the major peak in the corresponding N1s spectrum in Fig. 3a) along with a carbonaceous by-product (the major peak in the corresponding C1s spectrum in Fig. 3b). It

is noteworthy that the carbonaceous phase was not detected by the XRD analysis probably due to an amorphous or noncrystalline structure. Surprisingly, for $\text{Al}/\text{M} = 10$, a weak peak appears at 281.4 eV in the $\text{C}1\text{s}$ spectrum which is attributed to the $\text{Al}-\text{C}$ bond [33]. This suggests that at $\text{Al}/\text{M} > 6$, Al reacts with both C and N atoms resulting to the formation of an aluminum carbonitride phase; i.e. $\text{Al}_{10}\text{C}_1\text{N}_9$. Aluminum nitride is thermodynamically more stable than other aluminum compounds, such as AlH_3 and Al_4C_3 . Hence, for Al contents lower than the stoichiometric ratio, in which sufficient quantities of nitrogen are available, Al particles preferably react with N atoms to form the AlN phase. When a limited amount of nitrogen is available ($\text{Al}/\text{M} > 6$), the Al particles may react with C species. However, the carbide formation is also constrained by the low thermodynamic affinity of Al towards the C atoms and, consequently, the residual Al particles remain unreacted in the final milling products. This interpretation is corroborated by the Al peak observed in the XRD pattern of the system with $\text{Al}/\text{M} = 10$, as observed in Fig.1.

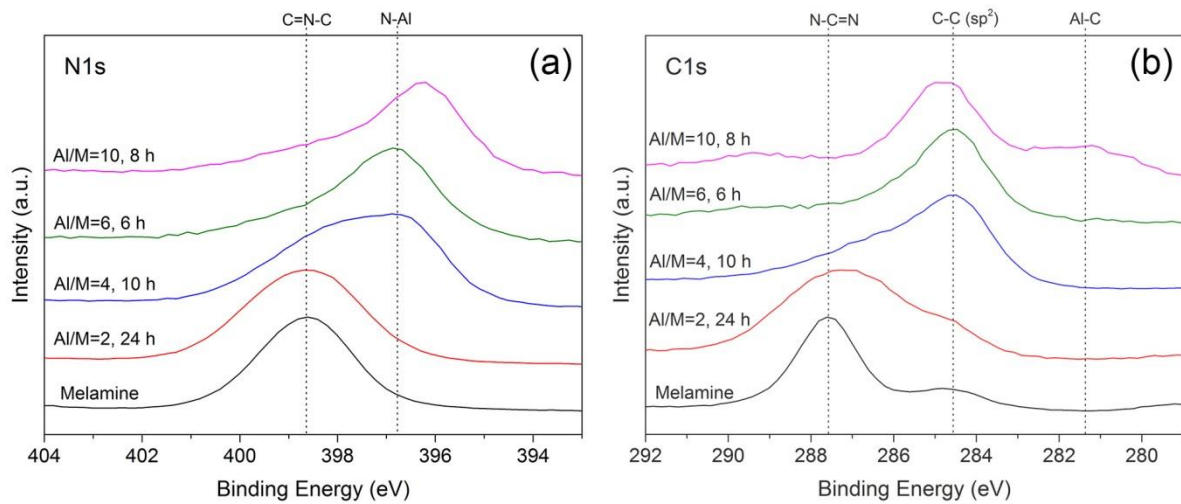


Figure 3. a) $\text{N}1\text{s}$ and b) $\text{C}1\text{s}$ spectra of melamine and milling products with different Al/M ratios milled for various times.

In order to obtain further information about the carbonaceous by-product, Raman spectroscopy was conducted on the powder mixture with Al/M = 6 milled for 6 h. Figure 4a shows two distinct peaks corresponding to the so-called D (defect) and G (graphitic) bands. The D feature reflects the disordered structure in graphite or any conjugated aromatic systems with more than 6 fused carbon rings [34]. The G band corresponds to the E_{2g} mode of graphite which generates by the in-plane bond-stretching motion of the pairs of sp^2 carbon atoms [35]. The spectrum, in overall, presents the main Raman features of the activated carbon materials [36]. The intense D band is related to the high level of disordering in the synthesized carbon phase. The valley between D and G bands refers to the small sp^2 clusters of 3-5 fused aromatic rings, typically found in the amorphous carbon materials [34, 37].

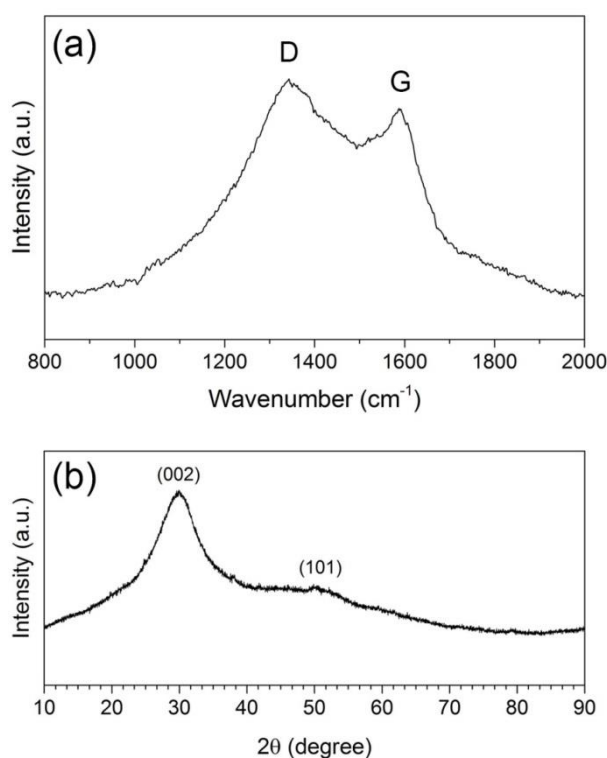


Figure 4. a) Raman spectrum of the powder mixture with Al/M = 6 milled for 6 h, b) XRD pattern of the same sample after two-step NaOH-HCl leaching treatment.

Further characterization of carbonaceous phase was carried out by XRD analysis. As mentioned previously, a two-step NaOH-HCl leaching treatment was conducted on the as-synthesized powder ($\text{Al/M} = 6$ and milled for 6 h) to remove AlN particles. Then, the final black residue was characterized by the XRD analysis. As shown in Fig. 4b, the AlN diffraction peaks were entirely vanished from the pattern, however, a very broad peak appears in the range of $22\text{--}35^\circ$. This peak with a weak shoulder at about 52° are indexed to (002) and (101) planes of carbon, respectively. The broad diffraction peak of carbon is indicative of the amorphous nature of the synthesized phase which is in good accordance with the results of Raman analysis.

A typical TEM image of the products milled for 6 h with $\text{Al/M} = 6$ is also presented in Fig. 5a. The as-milled powder shows fine particles with the irregular shapes consisting of the aggregated nanometric AlN and carbonaceous phases. HRTEM image of the carbonaceous phase leached from the same sample is presented in Fig. 5b. The image reveals that the carbonaceous phase is highly disordered. Moreover, the amorphous structure of this phase is confirmed by the diffuse ring observed in the corresponding inset fast Fourier transform (FFT) diffraction pattern.

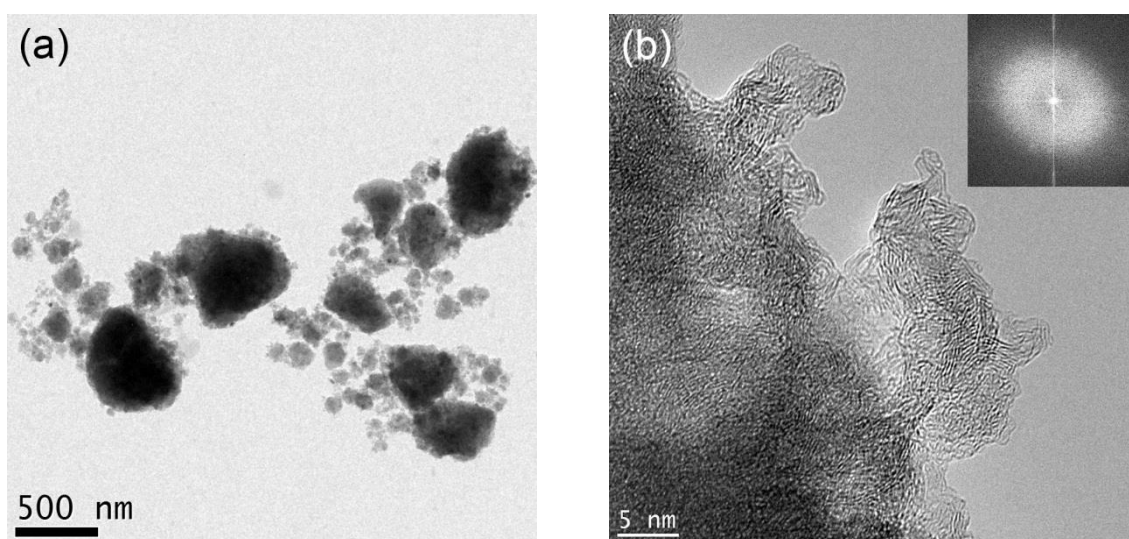
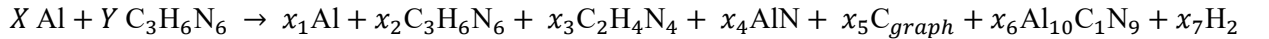


Figure 5. a) TEM image of the powder mixture with Al/M = 6 milled for 6 h b) HRTEM and inset FFT diffraction pattern of the same sample after leaching process.

To understand and corroborate the experimental results, we propose a simplified theoretical model of the experiment. We assume, for simplicity, that only the following reaction products are present in the experiment: aluminium (Al), melamine ($C_3H_6N_6$), 2-cyanoguanidine ($C_2H_4N_4$), aluminium nitride (AlN), graphene (as a carbon product, C_{graph}), carbon doped aluminium nitride ($Al_{10}C_1N_9$) and hydrogen gas (H_2). Although more products can be probably imagined to be formed, we choose only the above mentioned ones which can be clearly observed in the experiments. It is supposed that these products play an important role in the most relevant reactions. We choose graphene as example carbon product due to the easily formation of such flakes. One could opt to use graphite instead, or a complex mixture of carbonaceous materials, but this does not significantly change the qualitative behaviour of the model, as observed in the calculations by the use of graphite.

Using these products, a general reaction in the experiment can be written in the following form:



Here X and Y indicate the mole fractions of the initial precursors, while the x_i represents the final mole fractions of the products. The unknown x_i s must satisfy the following boundary conditions: (1) $\forall x_i \geq 0$ and (2) the total number of atoms related to each species should not change due to the reaction. Taking these into account, a finite phase space of possible sets of (x_1, \dots, x_7) can be defined. In this phase space, it is possible to calculate the reaction energy for each point, making use of calculated ab initio ground state energies (Table 1).

If an experiment was performed at zero kelvin and pressure, then, the configuration (x_1, \dots, x_7) at the minimum energy would be the one to be expected in that experiment. However, as an experiment is performed at finite temperature (or in this case finite energy introduced into the system due to the ball-milling) and pressure, it is to be expected that a significant fraction of

the phase space will be sampled. To include this behaviour in our model, we sampled the phase space using a Boltzmann distribution, giving a weight:

$$\frac{N_i}{N} = \frac{e^{-\frac{E_i}{k_B T}}}{\sum_j e^{-\frac{E_j}{k_B T}}}$$

to the i^{th} configuration (x_1, \dots, x_7) of the phase space. Since the required energy is provided through the ball-milling, we replace the term $k_B T$ by E_{exp} which represents the energy from the ball-milling. The milling energy was estimated by a method described in [38, 39] and input energy was calculated to be of the order of 125.5 J/(g.s) or 35 meV/s. As a result, the configuration (x_1, \dots, x_7) of the reaction is the ensemble average over the phase space.

Table 1. Calculated ab initio ground state energies for various products.		
material	Energy (eV)	Description
Fcc Al	-3.766	per Al atom
Melamine	-100.218	per molecule
2-cyanoguanidine	-65.491	per molecule
AlN	-14.893	per formula unit (1Al+1N)
graphene	-9.227	per C atom
Al ₁₆ C ₁ N ₁₅	-146.495	Energy scaled to a cell containing 10 Al atoms (20 atoms total)
Al ₈ C ₁ N ₇	-144.100	Energy scaled to a cell containing 10 Al atoms (20 atoms total)
Al ₁₀ C ₁ N ₉	-145.058	Interpolated from Al ₁₆ C ₁ N ₁₅ and Al ₈ C ₁ N ₇
H ₂	-2.236	per molecule

In Fig. 6, the mass-fraction of the configurations (x_1, \dots, x_7) as a function of the mole fraction of Al (X) is shown. This already presents a reasonable qualitative agreement with the experiments. At low Al fractions, melamine is not fully consumed for the AlN formation and partially dissociates to 2-cyanoguanidine. Also, the formation of a considerable quantity of carbon-based product is confirmed as well as C doped AlN (Al₁₀C₁N₉). For a higher energy E_{exp} , the fraction of 2-cyanoguanidine increases significantly, as well as the fraction of Al₁₀C₁N₉. Although the former is favourable, the latter is not desired for Al fractions below 50

mol. %. Furthermore, for high Al concentrations, the fraction of $\text{Al}_{10}\text{C}_1\text{N}_9$ should exceed that of the undoped AlN.

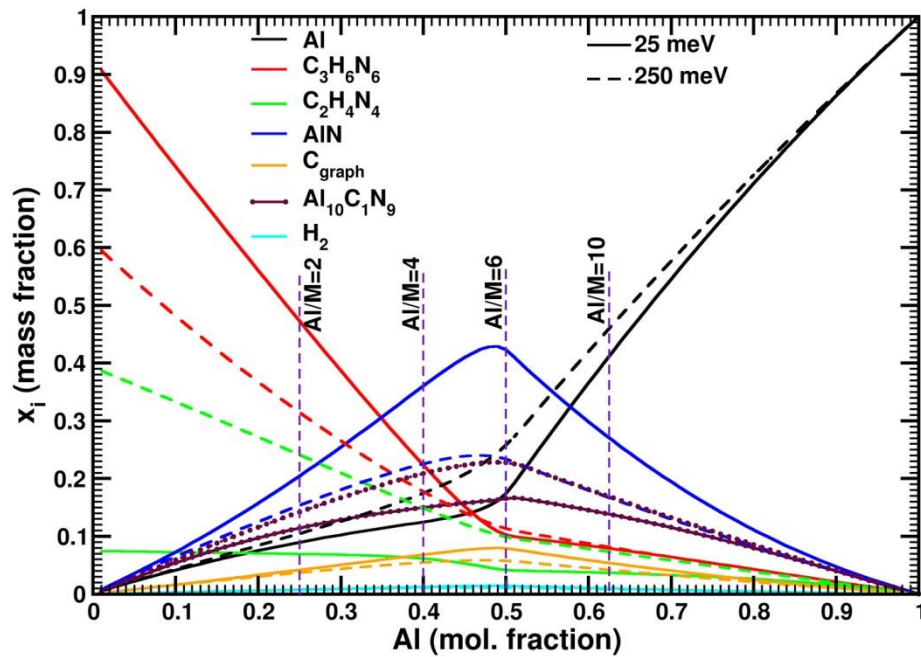


Figure 6. Mass fraction of the different products as a function of the initial Al fraction.

At this point, it is important to remember that during the reaction presented above, 2-cyanoguanidine can be also assumed as a nitrogen source for the formation of AlN. In addition, the formed graphene provides a source for the formation of C doped AlN. Finally, one could also imagine at low Al concentrations, the melamine molecules to break down into 2-cyanoguanidine under the impacts of the steel balls without formation of AlN. This proposes three possible secondary reactions to consider in our model:

- 1) $X \text{ Al} + Y \text{ C}_2\text{H}_4\text{N}_4 \rightarrow x_1^b \text{ Al} + x_3^b \text{ C}_2\text{H}_4\text{N}_4 + x_4^b \text{ AlN} + x_5^b \text{ C}_{\text{graph}} + x_6^b \text{ Al}_{10}\text{C}_1\text{N}_9 + x_7^b \text{ H}_2$
- 2) $X \text{ Al} + Y \text{ AlN} + Z \text{ C}_{\text{graph}} \rightarrow x_1^c \text{ Al} + x_4^c \text{ AlN} + x_5^c \text{ C}_{\text{graph}} + x_6^c \text{ Al}_{10}\text{C}_1\text{N}_9$
- 3) $X \text{ C}_3\text{H}_6\text{N}_6 \rightarrow x_2^d \text{ C}_3\text{H}_6\text{N}_6 + x_3^d \text{ C}_2\text{H}_4\text{N}_4$

It should be noted that these are simplified reactions which are intended to rationalize experimental observations. Furthermore, the ball-milling experiment can be seen as the impacts of steel balls on melamine molecules and Al particles which provide the required energy for

AlN formation. If we assume the energy of an impact is equally distributed over all atoms involved in the reaction, then it is important to note that an Al particle contains many more atoms than a melamine molecule. Assuming a spherical particle radius of 4 nm, a volume of 268 nm³ is calculated. The volume per atom for fcc Al is 16.42 Å³, while that for AlN and AlN_{1-x}C_x (x<0.125) is about 10.59-10.84 Å³, giving rise to about 16×10^3 Al atoms in the particle, or 25×10^3 atoms in an AlN particle. Based on these values, we can introduce a weighting factor for the E_{exp} in the Boltzmann factor linked to each specific reaction, as demonstrated in Table 2.

Table 2. Estimation of energy weighting factors for various reactions during milling.					
Reaction	Initial products	Estimate of atoms		Atom factor	Energy weighting factor
Primary	Al + C ₃ H ₆ N ₆	$16 \times 10^3 + 15$	$= 16 \times 10^3$	1	1
melamine degeneration	C ₃ H ₆ N ₆	15	$= 15$	1/1000	1000
2-cyanoguanidine reaction	Al + C ₂ H ₄ N ₄	$16 \times 10^3 + 10$	$= 16 \times 10^3$	1	1
carbon reaction	(AlN + Al) + C	$25 \times 10^3 +$ ~100	$= 25 \times 10^3$	3/2	2/3

Combining the four reactions and the weighted E_{exp} for the Boltzmann factors, our model shows good qualitative agreement with the observations in the experiment (shown in Fig. 7). The energy of ball-milling in the experiments can be calculated to be of the order of 35 meV/sec.

At high Al fractions, the proportion of C doped fraction ($\text{Al}_{10}\text{C}_1\text{N}_9$) clearly exceeds the undoped AlN fraction, while at low Al content, a significant fraction of 2-cyanoguanidine is expected to be formed. At stoichiometry, the AlN fraction dominates, as long as E_{exp} is not too large. However, one should bear in mind that although $\text{Al}_{10}\text{C}_1\text{N}_9$ is almost as stable as AlN, the formation energy of the C defect itself is rather high [40]. Therefore, this could be a rate limiting factor which lowers the fraction of $\text{Al}_{10}\text{C}_1\text{N}_9$ in favour of the AlN fraction. A second limitation of our model is the fact that time is not an explicit parameter in our model. This would probably give rise to an increase of the 2-cyanoguanidine fraction, as well as the $\text{Al}_{10}\text{C}_1\text{N}_9$ fraction. In the other words the latter limitation may partially compensate the effect of the inclusion of the C defect formation energy. This interpretation is in line with the experiments which show longer milling times (and consequently higher input energy) are required for the reaction completion at non stoichiometric Al/M ratios.

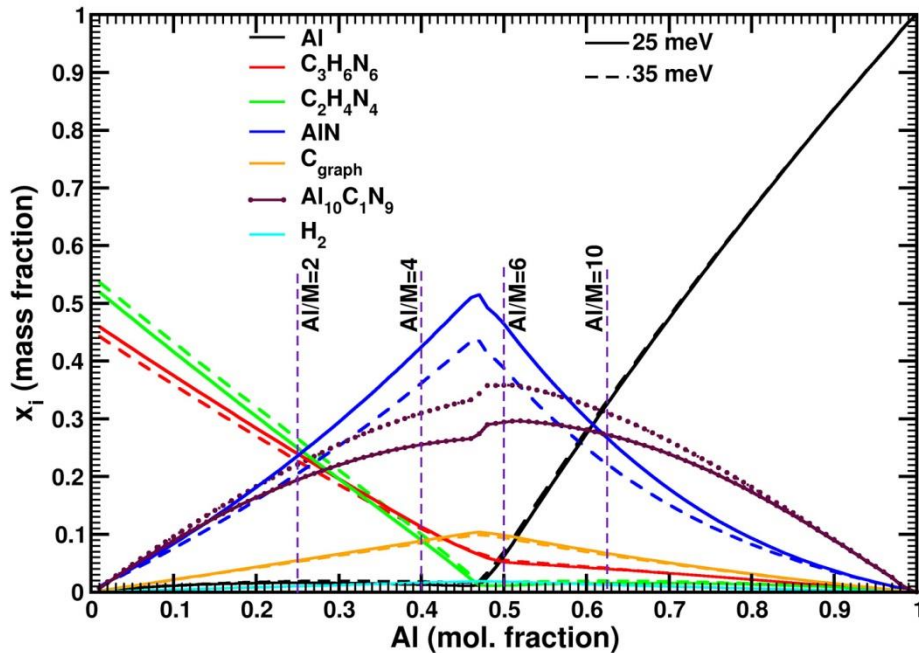


Figure 7. Mass fraction of the different products as function of the initial Al fraction for a model including several reactions and weighted energy factors.

Despite these limitations, our simple model is able to elucidate the experimental observations:

1) **Al/M = 2:** Al is the limiting factor in the reaction, and is expected to be almost entirely transformed to AlN and (to lesser extend) $\text{Al}_{10}\text{C}_1\text{N}_9$. Interaction of the remaining melamine with the steel balls leads to a degradation of the melamine into 2-cyanoguanidine.

2) **Al/M = 4, 6:** A large fraction of AlN is formed, as well as a significant fraction of carbonaceous material. Also, a small fraction of melamine remains unreacted. It is interesting to note that the optimum formation of AlN is not found at the exact stoichiometry, but slightly below (at 47 at. %). From our models, we have found this behaviour arises as soon as the phase space of possible configurations is sampled. The formation of the 2-cyanoguanidine side-product prevents some of the N to be consumed in the formation of AlN, while the formation of C-doped AlN consumes some of the AlN. The combination of these 2 side-reactions and their contribution to the possible configurations in the phase space of the theoretical models, result in the slight shift of the optimum formation of AlN.

3) **Al/M = 10:** For Al fractions of 50 at.% and higher, the $\text{Al}_{10}\text{C}_1\text{N}_9$ becomes dominant.

Bringing all experimental and theoretical data together, the overall reaction pathways for the systems with different Al/M ratios are realized. As schematically illustrated in Fig. 8, the reaction at $\text{Al/M} < 6$ is mainly governed by the dissociation of melamine along with the formation of 2-cyanoguanidine and AlN. The proportion of 2-cyanoguanidine to AlN remarkably decreases with the increase of Al/M ratio. At the stoichiometric ratio ($\text{Al/M} = 6$), the Al particles entirely react with N atoms of the organic precursor and the final product consists of AlN together with an amorphous carbonaceous material. The 2-cyanoguanidine is gradually substituted by the heterogeneous carbon phase when the Al content increases. As known, 2-cyanoguanidine is a melamine fragment, while the heterogeneous carbon phase is formed during polymerization of the melamine molecules [24]. Therefore, one may conclude

that the overall reaction mechanism is governed by the ratio of the reactants and varies from dissociation to polymerization of melamine with the increase of Al/M ratio. For $\text{Al/M} > 6$, i.e., when the Al content is higher than the stoichiometric ratio, Al particles react with both N and C constituents of the organic precursor to form the $\text{Al}_{10}\text{C}_1\text{N}_9$ phase. However, since aluminum has a higher affinity to react with nitrogen than carbon, the final structure ($\text{Al}_{10}\text{C}_1\text{N}_9$) is assumed to be a nitrogen-rich carbonitride phase. This hypothesis is supported by the XRD and XPS analyses (the spectra corresponding to $\text{Al/M} = 10$ in Figs. 1 and 3), which demonstrate the presence of intact Al and C constituents (in the form of metallic Al and a carbonaceous phase) in the final products, while the N atoms have been fully consumed by the Al particles. These results suggest the optimized conditions for the synthesis of AlN. According to the above-mentioned findings, if AlN synthesis is the aim, then the Al/M ratio should be 6, while at lower and higher Al/M ratios, the main products are 2-cyanoguanidine and $\text{Al}_{10}\text{C}_1\text{N}_9$, respectively.

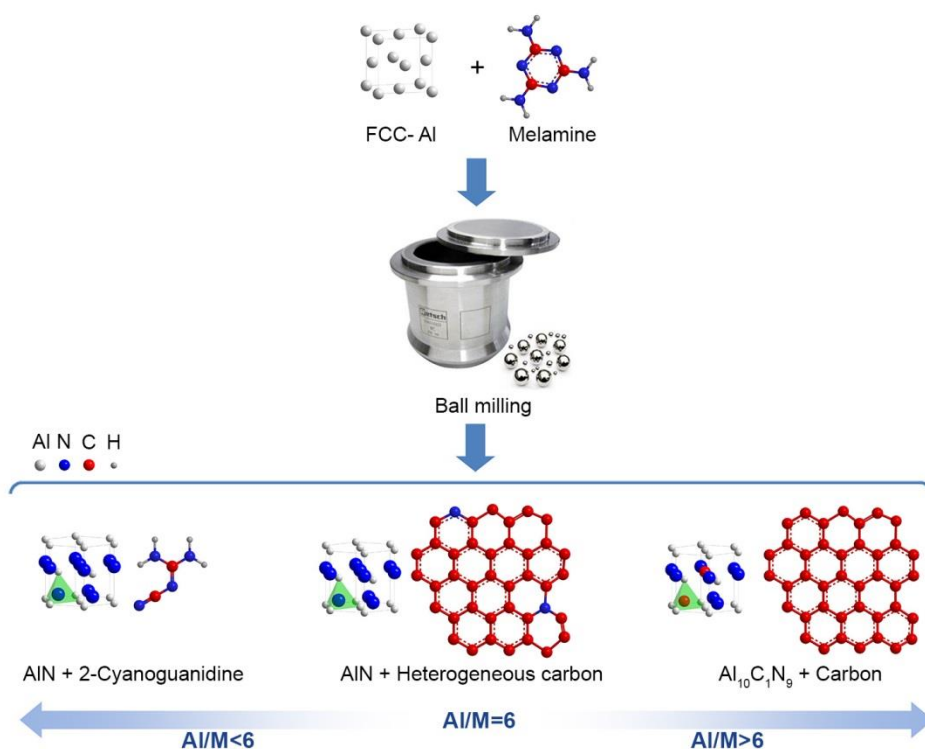


Figure 8. Schematic illustration of the milling products as a function of the A/M reactant ratio.

4. Conclusions

The mechanochemical reaction of Al with melamine at different reactant ratios was studied from both theoretical and experimental points of views. The results demonstrated that the products varied from AlN and 2-cyanoguanidine towards $\text{Al}_{10}\text{C}_1\text{N}_9$ and carbon phase proportional to the Al/M ratio. For Al/M ratios less than the stoichiometric value, the reaction mechanism was mainly governed by the dissociation of melamine and subsequent formation of fragments, such as 2-cyanoguanidine, while the polymerization of melamine was more pronounced at higher Al/M ratios. At the stoichiometric ratio, the Al particles entirely reacted with the nitrogen atoms of the melamine molecules which in turn, led to the formation of nanostructured AlN along with a heterogeneous carbon structure. According to these findings, carbon atoms in the carbonaceous phase partially participated in the reaction, in particular, when the Al content exceeded the stoichiometric ratio ($\text{Al/M} > 6$), where the formation of $\text{Al}_{10}\text{C}_1\text{N}_9$ phase prevailed.

Acknowledgements

S.A.R. gratefully acknowledges funding and support from IFW Dresden. D.E.P.V. acknowledges funding by the Foundation of Scientific Research-Flanders (FWO) (project no. 12S3415N). The computational resources and services used in this work were provided by the VSC (Flemish Supercomputer Center), funded by the Research Foundation - Flanders (FWO) and the Flemish Government – department EWI. D.E.P.V. wishes to acknowledge B. Cleuren for the interesting discussion on ensemble theory.

5. References

- [1] Y. Lu, S. Ozcan, Green nanomaterials: On track for a sustainable future, *Nano Today* 10(4) (2015) 417-420.
- [2] S.L. James, C.J. Adams, C. Bolm, D. Braga, P. Collier, T. Friscic, F. Grepioni, K.D.M. Harris, G. Hyett, W. Jones, A. Krebs, J. Mack, L. Maini, A.G. Orpen, I.P. Parkin, W.C. Shearouse, J.W. Steed, D.C. Waddell, Mechanochemistry: opportunities for new and cleaner synthesis, *Chem. Soc. Rev.* 41(1) (2012) 413-447.
- [3] P. Balaz, M. Achimovicova, M. Balaz, P. Billik, Z. Cherkezova-Zheleva, J.M. Criado, F. Delogu, E. Dutkova, E. Gaffet, F.J. Gotor, R. Kumar, I. Mitov, T. Rojac, M. Senna, A. Streletskii, K. Wieczorek-Ciurowa, Hallmarks of mechanochemistry: from nanoparticles to technology, *Chem. Soc. Rev.* 42(18) (2013) 7571-7637.
- [4] J. Xu, J. Shui, J. Wang, M. Wang, H.-K. Liu, S.X. Dou, I.-Y. Jeon, J.-M. Seo, J.-B. Baek, L. Dai, Sulfur–Graphene Nanostructured Cathodes via Ball-Milling for High-Performance Lithium–Sulfur Batteries, *ACS Nano* 8(10) (2014) 10920-10930.
- [5] V. León, A.M. Rodriguez, P. Prieto, M. Prato, E. Vázquez, Exfoliation of graphite with triazine derivatives under ball-milling conditions: preparation of few-layer graphene via selective noncovalent interactions, *ACS Nano* 8(1) (2013) 563-571.
- [6] I.-Y. Jeon, S.-Y. Bae, J.-M. Seo, J.-B. Baek, Scalable Production of Edge-Functionalized Graphene Nanoplatelets via Mechanochemical Ball-Milling, *Adv. Funct. Mater.* 25(45) (2015) 6961-6975.
- [7] G.-W. Wang, Mechanochemical organic synthesis, *Chem. Soc. Rev.* 42(18) (2013) 7668-7700.
- [8] L. Takacs, The historical development of mechanochemistry, *Chem. Soc. Rev.* 42(18) (2013) 7649-7659.
- [9] M.T. Hardy, D.F. Feezell, S.P. DenBaars, S. Nakamura, Group III-nitride lasers: a materials perspective, *Mater. Today* 14(9) (2011) 408-415.

- [10] L.C. Pathak, A.K. Ray, S. Das, C.S. Sivaramakrishnan, P. Ramachandrarao, Carbothermal synthesis of nanocrystalline aluminum nitride powders, *J. Am. Ceram. Soc.* 82(1) (1999) 257-260.
- [11] Y. Baik, R.A.L. Drew, Aluminum nitride: Processing and applications, *Key Eng. Mater.* 122 (1996) 553-570.
- [12] B.M. Eick, J.P. Youngblood, Carbothermal reduction of metal-oxide powders by synthetic pitch to carbide and nitride ceramics, *J. Mater. Sci.* 44(5) (2009) 1159-1171.
- [13] B. Mazumder, A.L. Hector, Synthesis and applications of nanocrystalline nitride materials, *J. Mater. Chem.* 19(27) (2009) 4673-4686.
- [14] M.A. Khan, M. Shatalov, H.P. Maruska, H.M. Wang, E. Kuokstis, III-nitride UV devices, *Jpn. J. Appl. Phys.* 44(10) (2005) 7191-7206.
- [15] Y. Taniyasu, M. Kasu, T. Makimoto, An aluminium nitride light-emitting diode with a wavelength of 210 nanometres, *Nature* 441(7091) (2006) 325-328.
- [16] A. Calka, J.I. Nikolov, Direct synthesis of AlN and Al-AlN composites by room temperature magneto ball milling: the effect of milling condition on formation of nanostructures, *Nanostruct. Mater.* 6 (1995) 409-412.
- [17] P. Li, S. Xi, J. Zhou, Phase transformation and gas-solid reaction of Al_2O_3 during high-energy ball milling in N_2 atmosphere, *Ceram. Int.* 35(1) (2009) 247-251.
- [18] Y. Du, M. Lei, H. Yang, Facile solid-state synthesis route to metal nitride nanoparticles, *J. Mater. Sci. Technol.* 24(5) (2008) 737-741.
- [19] M. Lei, H.Z. Zhao, H. Yang, B. Song, L.Z. Cao, P.G. Li, W.H. Tang, Syntheses of metal nitrides, metal carbides and rare-earth metal dioxymonocarbodiimides from metal oxides and dicyandiamide, *J. Alloys Compd.* 460(1-2) (2008) 130-137.
- [20] H. Zhao, M. Lei, X. Chen, W. Tang, Facile route to metal nitrides through melamine and metal oxides, *J. Mater. Chem.* 16 (2006) 4407-4407.

- [21] S.A. Rounaghi, A.R.K. Rashid, H. Eshghi, J.V. Khaki, Formation of nanocrystalline h-AlN during mechanochemical decomposition of melamine in the presence of metallic aluminum, *J. Solid State Chem.* 190 (2012) 8-11.
- [22] S.A. Rounaghi, H. Eshghi, A.R.K. Rashid, J.V. Khaki, M.S. Khoshkhoo, S. Scudino, J. Eckert, Synthesis of nanostructured AlN by solid state reaction of Al and diaminomaleonitrile, *J. Solid State Chem.* 198 (2013) 542-547.
- [23] J.F. Sun, M.Z. Wang, Y.C. Zhao, X.P. Li, B.Y. Liang, Synthesis of titanium nitride powders by reactive ball milling of titanium and urea, *J. Alloys Compd.* 482(1-2) (2009) L29-L31.
- [24] S.A. Rounaghi, H. Eshghi, S. Scudino, A. Vyalikh, D.E.P. Vanpoucke, W. Gruner, S. Oswald, A.R. Kiani Rashid, M. Samadi Khoshkhoo, U. Scheler, J. Eckert, Mechanochemical route to the synthesis of nanostructured Aluminium nitride, *Sci. Rep.* 6 (2016) 33375.
- [25] H.D. Li, G.T. Zou, H. Wang, H.B. Yang, D.M. Li, M.H. Li, S. Yu, Y. Wu, Z.F. Meng, Synthesis and infrared study of nanosized aluminum nitride powders prepared by direct current arc plasma, *J. Phys. Chem. B* 102(44) (1998) 8692-8695.
- [26] L. Yate, J.C. Caicedo, A.H. Macias, F.J. Espinoza-Beltrán, G. Zambrano, J. Muñoz-Saldaña, P. Prieto, Composition and mechanical properties of AlC, AlN and AlCN thin films obtained by r.f. magnetron sputtering, *Surf. Coat. Technol.* 203(13) (2009) 1904-1907.
- [27] N. Hellgren, R.T. Haasch, S. Schmidt, L. Hultman, I. Petrov, Interpretation of X-ray photoelectron spectra of carbon-nitride thin films: New insights from in situ XPS, *Carbon* 108 (2016) 242-252.
- [28] D.L. Yu, J.L. He, Z.Y. Liu, B. Xu, D.C. Li, Y.J. Tian, Phase transformation of melamine at high pressure and temperature, *J. Mater. Sci.* 43(2) (2008) 689-695.

- [29] L. Rosenberger, R. Baird, E. McCullen, G. Auner, G. Shreve, XPS analysis of aluminum nitride films deposited by plasma source molecular beam epitaxy, *Surf. Interface Anal.* 40(9) (2008) 1254-1261.
- [30] H. Liu, D.C. Bertolet, J.W. Rogers Jr, The surface chemistry of aluminum nitride MOCVD on alumina using trimethylaluminum and ammonia as precursors, *Surf Sci.* 320(1–2) (1994) 145-160.
- [31] A.P. Dementjev, A. de Graaf, M.C.M. van de Sanden, K.I. Maslakov, A.V. Naumkin, A.A. Serov, X-Ray photoelectron spectroscopy reference data for identification of the C₃N₄ phase in carbon–nitrogen films, *Diamond Relat. Mater.* 9(11) (2000) 1904-1907.
- [32] J.C. Lascovich, R. Giorgi, S. Scaglione, Evaluation of the sp²/sp³ ratio in amorphous carbon structure by XPS and XAES, *Appl. Surf. Sci.* 47(1) (1991) 17-21.
- [33] J. Ning, S. Xu, K.N. Ostrikov, C. Jianwei, L. Yinan, K. Mei Ling, S. Lee, Synthesis and structural properties of Al-C-N-O composite thin films, *Thin Solid Films* 385(1–2) (2001) 55-60.
- [34] X. Li, J.-i. Hayashi, C.-Z. Li, FT-Raman spectroscopic study of the evolution of char structure during the pyrolysis of a Victorian brown coal, *Fuel* 85(12–13) (2006) 1700-1707.
- [35] M.S. Dresselhaus, A. Jorio, M. Hofmann, G. Dresselhaus, R. Saito, Perspectives on carbon nanotubes and graphene raman spectroscopy, *Nano Letters* 10(3) (2010) 751-758.
- [36] N. Shimodaira, A. Masui, Raman spectroscopic investigations of activated carbon materials, *J. Appl. Phys.* 92(2) (2002) 902-909.
- [37] J. McDonald-Wharry, M. Manley-Harris, K. Pickering, Carbonisation of biomass-derived chars and the thermal reduction of a graphene oxide sample studied using Raman spectroscopy, *Carbon* 59 (2013) 383-405.
- [38] M. Buzaglo, I.P. Bar, M. Varenik, L. Shunak, S. Pevzner, O. Regev, Graphite-to-Graphene: Total Conversion, *Adv. Mater.* 29(8) (2017) 1603528.

- [39] N. Burgio, A. Iasonna, M. Magini, S. Martelli, F. Padella, Mechanical alloying of the Fe–Zr system. Correlation between input energy and end products, *Il Nuovo Cimento D* 13(4) (1991) 459-476.
- [40] S.A. Rounaghi, D.E.P. Vanpoucke, H. Eshghi, S. Scudino, E. Esmaeili, S. Oswald, J. Eckert, Mechanochemical synthesis of nanostructured metal nitrides, carbonitrides and carbon nitride: a combined theoretical and experimental study, *PCCP* 19(19) (2017) 12414-12424.

Table captions

Table 1. Calculated ab initio ground state energies for various products.

Table 2. Estimation of energy weighting factors for various reactions during milling.

Figure captions

Figure 1. XRD patterns of the powder mixtures with Al/M ratios of a) 2, b) 4, c) 6 and d) 10 milled for various times.

Figure 2. FTIR spectra of a) melamine and milling products with Al/M ratios of b) 2, c) 4, d) 6 and e) 10 milled for 24, 10, 6 and 8 h, respectively.

Figure 3. a) N1s and b) C1s spectra of melamine and milling products with different Al/M ratios milled for various times.

Figure 4. a) Raman spectrum of the powder mixture with $\text{Al/M} = 6$ milled for 6 h, b) XRD pattern of the same sample after two-step NaOH-HCl leaching treatment.

Figure 5. a) TEM image of the powder mixture with $\text{Al/M} = 6$ milled for 6 h b) HRTEM and inset FFT diffraction pattern of the same sample after leaching process.

Figure 6. Mass fraction of the different products as function of the initial Al fraction.

Figure 7. Mass fraction of the different products as function of the initial Al fraction for a model including several reactions and weighted energy factors.

Figure 8. Schematic illustration of the milling products as a function of the A/M reactant ratio.